View metadata, citation and similar papers at core.ac.uk

brought to you by CORE

provided by Diposit Digital de la Universitat de Barcelona

Journal of Electroanalytical Chemistry xxx (xxxx) xxx–xxx

Contents lists available at ScienceDirect

Journal of Electroanalytical Chemistry

journal homepage: www.elsevier.com/locate/jelechem

On-site H_2O_2 electrogeneration at a CoS_2-based air-diffusion cathode for the electrochemical degradation of organic pollutants

Carlota Ridruejo[a], Francisco Alcaide[b,*], Garbiñe Álvarez[b], Enric Brillas[a], Ignasi Sirés[a,*]

[a] Laboratori d'Electroquímica dels Materials i del Medi Ambient, Departament de Química Física, Facultat de Química, Universitat de Barcelona, Martí i Franquès 1-11, 08028 Barcelona, Spain

[b] Materials for Energy Unit, Energy Storage Area, IK4-CIDETEC, Paseo Miramón 196, 20014 San Sebastián, Spain

ARTICLE INFO

Keywords:
CoS_2
EAOPs
Hydrogen peroxide
Gas-diffusion electrode
Oxygen reduction reaction
Tetracaine

ABSTRACT

This work reports, for the first time, the manufacture and use of an air-diffusion cathode containing CoS_2 nanoparticles to enhance the H_2O_2 electrogeneration. Hydrothermal synthesis allowed the formation of crystalline CoS_2 with pyrite structure, either unsupported or supported on carbon nanotubes. Both kinds of catalysts were characterized by X-ray diffraction and FE-SEM combined with energy dispersive X-ray analysis. The use of carbon nanotubes as support led to a remarkable enhancement of the CoS_2 stability, as deduced from cyclic voltammetry analysis. The electrochemical activity of the CoS_2-based materials towards the oxygen reduction reaction (ORR) in acidic medium was examined by potentiodynamic techniques using a rotating disk electrode. Both catalysts showed activity towards the ORR, being predominant the two-electron pathway to form H_2O_2 as main product. A novel CoS_2-on-carbon nanotubes catalyzed air-diffusion cathode, as well as an uncatalyzed one made for comparison, was manufactured to electrogenerate H_2O_2 under galvanostatic conditions in an undivided two-electrode cell. A concentration of 56.9 mM was found with the former cathode at 100 mA cm^{-2}, much > 32.0 mM found with the uncatalyzed cathode. This informs about the high performance of the CoS_2 nanoparticles to promote the two-electron ORR. Finally, the treatment of aqueous solutions of the anaesthetic tetracaine at pH 3.0 and 100 mA cm^{-2} by electro-oxidation and photoelectro-Fenton processes demonstrated the viability of the manufactured CoS_2-based cathode for water treatment.

1. Introduction

Hydrogen peroxide is a versatile, powerful, green oxidant that can be directly used in a large number of industrial applications. Its further activation to yield hydroxyl radicals (˙OH) gives rise to the so-called H_2O_2-based advanced oxidation processes (AOPs), which show great performance for the transformation of toxic, (bio)refractory pollutants into innocuous by-products. H_2O_2 can be activated by UV [1] and metal catalysts like Fe^{2+} [2], as well as at high temperature and pressure in hot AOPs. Currently, the most widespread method for H_2O_2 production at large scale is the anthraquinone cyclic process, although emerging alternatives have been recently developed [3]. Among them, the electrochemical approach based on the two-electron oxygen reduction reaction (ORR) (1) at a suitable cathode has gained interest owing to its versatility. This process may occur at low overvoltage and in homogeneous environment.

$$O_2 + 2\,H^+ + 2e^- \rightarrow H_2O_2 \quad (1)$$

Since the first electrosynthesis of H_2O_2 in 1882 [4], two main setups have prevailed depending on the mode of air/O_2 supply: direct sparging into the solution or feeding through a gas-diffusion electrode (GDE). In the former arrangement, large surface area carbonaceous materials like carbon fibers [5], carbon/graphite felt and reticulated vitreous carbon [6–9] have been used. However, the limited solubility and slow mass transport of O_2 in water impede the production of great concentrations of H_2O_2. The use of GDEs allows overcoming these drawbacks, thanks to their porous structure and the coexistence of a triple phase boundary (TPB) [10–14]. The use of divided cells significantly enhances the production of H_2O_2 [4].

Despite the high current efficiency of raw GDEs, further progress is envisaged from the substitution of commercial, unmodified cathodes based on active carbon or carbon black by novel engineered materials with nanocarbons like carbon nanotubes (CNTs) as support. They may show higher ability to reach higher current values at lower overvoltage, thus enhancing the ORR kinetics and diminishing the energy demand. For example, greater selectivity for the two-electron ORR has been

* Corresponding authors.
E-mail addresses: falcaide@cidetec.es (F. Alcaide), i.sires@ub.edu (I. Sirés).

http://dx.doi.org/10.1016/j.jelechem.2017.09.010
Received 3 April 2017; Received in revised form 24 August 2017; Accepted 6 September 2017
1572-6657/ © 2017 Elsevier B.V. All rights reserved.

Please cite this article as: Ridruejo, C., Journal of Electroanalytical Chemistry (2017), http://dx.doi.org/10.1016/j.jelechem.2017.09.010

found using GDEs modified with Ta_2O_5 particles [15] and Co(II) phthalocyanine [16,17]. Cobalt-based materials in the form of chalcogenides (late transition metal chalcogenides, LTMCs [18]), oxides or Co nanoparticles are among the most active electrocatalysts for promoting the desired ORR pathway in acidic medium [19]. Therefore, non-precious metal-based electrocatalysts such as Co_xS_y could offer low-cost alternatives and, furthermore, if synthesized as CNTs hybrids they could attain the highest activity and stability among LTMCs. At the moment, CoS_2 nanocrystals with pyrite structure have been shown as extremely low cost catalysts suitable for both, hydrogen evolution reaction and the two-electron ORR with enough stability in acidic liquid electrolyte and in solid electrolyte like Nafion® [20], whereas long-standing durability of selenides is more questionable [21].

Electrochemical AOPs (EAOPs) have received increasing attention for wastewater treatment. Electrochemical oxidation (EO) is the simplest EAOP and consists in the in situ production of adsorbed hydroxyl radical (M(˙OH)) from water reduction at a large O_2-overvoltage anode (M) [22,23]. It has been found that boron-doped diamond (BDD) thin-films possess the largest oxidation ability when treating organic pollutants due to their greater O_2-overvoltage compared to other anodes and the low interaction with ˙OH, allowing the generation of large amounts of BDD(˙OH) that oxidize more effectively the organics [24,25]. The formation of this physisorbed radical can be written as follows [23]:

$$BDD + H_2O \rightarrow BDD(^{\bullet}OH) + H^+ + e^- \quad (2)$$

The application of EO in an electrochemical reactor equipped with a BDD anode and a GDE cathode gives rise to EO with electrogenerated H_2O_2 (EO-H_2O_2) process, being the organics destroyed pre-eminently by BDD(˙OH) and, to a much lesser extent, by reactive oxygen species (ROS) like H_2O_2 and hydroperoxyl radical ($HO_2^{\bullet}$), among others [26]. The oxidation ability of this procedure is strongly enhanced by the additional production of ˙OH in the bulk using Fenton-based EAOPs. In the electro-Fenton (EF) method, this radical is generated through Fenton's reaction (3) upon addition of Fe^{2+} catalyst to an acidic solution, which is continuously activated thanks to Fe^{2+} regeneration from cathodic Fe^{3+} reduction via reaction (4) [23]. The most powerful Fenton-based EAOP is photoelectro-Fenton (PEF) [23,27], in which the solution is also irradiated with UVA light to accelerate the degradation process by: (i) upgrading Fe^{2+} regeneration thanks to a larger ˙OH generation from the photolytic reduction of $Fe(OH)^{2+}$ species via reaction (5), and (ii) photodecomposing Fe(III) complexes with generated carboxylic acids via reaction (6).

$$H_2O_2 + Fe^{2+} \rightarrow Fe^{3+} + {}^{\bullet}OH + OH^- \quad (3)$$

$$Fe^{3+} + e^- \rightarrow Fe^{2+} \quad (4)$$

$$Fe(OH)^{2+} + h\nu \rightarrow Fe^{2+} + {}^{\bullet}OH \quad (5)$$

$$Fe(OOCR)^{2+} + h\nu \rightarrow Fe^{2+} + CO_2 + R^{\bullet} \quad (6)$$

In recent years, the presence of pharmaceuticals in the environment, in particular in water matrices, has caused global alarm due to their unknown, long-term effects on living beings [22,28]. H_2O_2-based EAOPs have demonstrated great ability to degrade traces of pharmaceuticals. Acidic aqueous solutions of antibiotics such as sulfachloropyridazine [29], sulfanilamide [30], amoxicillin [31], levofloxacin [32], norfloxacin [33] and erythromycin [34] have been removed by EO-H_2O_2, EF and PEF with air sparged into solution, whereas the antibiotic sulfamethazine [35], anti-inflammatory naproxen [36] and antidepressant fluoxetine [37] have been treated in electrolytic cells equipped with a GDE.

This paper reports the synthesis and characterization of several CoS_2-based catalysts, either unsupported or supported on functionalized carbon nanotubes (MWCNTs). The electrochemical activity of these materials towards the oxygen reduction reaction in acidic medium was examined in a three-electrode cell by means of potentiodynamic techniques. Furthermore, for the first time, GDEs containing CoS_2 powder have been manufactured. Worth noting, only a carbonaceous cathode material with Co_9S_8 as cobalt chalcogenide supported on graphitized carbon has been reported in the literature so far [38]. The ability of all novel GDEs to electrogenerate H_2O_2 has been studied at a lab-scale electrochemical reactor under potentiostatic and galvanostatic conditions. Finally, aqueous solutions of the anaesthetic tetracaine taken as a model pharmaceutical have been treated at pH 3.0 and constant current by EO-H_2O_2 and PEF using the best synthesized CoS_2-based GDEs.

2. Experimental

2.1. Chemicals

Commercial multiwall carbon nanotubes (MWCNTs) were supplied by Arkema (Graphistrength® C100) and Cheap Tubes Inc. (OD < 8 nm, L 10–30 μm, purity > 95 wt%, COOH content 3.86 wt%). Concentrated sulfuric and nitric acids, reagent grade, were purchased from Scharlau. Cobalt(II) chloride hexahydrate (Scharlau), sodium thiosulfate pentahydrate (Sigma-Aldrich) and sulfur (Sigma-Aldrich) were reagent grade. Nafion® perfluorinated resin solution 5 wt% was from Sigma-Aldrich and extra pure 2-propanol from Scharlau. Anhydrous sodium sulfate used as background electrolyte and concentrated sulfuric acid for adjusting solution pH, both reagent grade, were supplied by Prolabo and Merck, respectively. Iron(II) sulfate heptahydrate used as catalyst was purchased from Fluka. Tetracaine hydrochloride (> 99% purity) was purchased from Sigma-Aldrich. Organic solvents and other chemicals were of HPLC or analytical grade from Sigma-Aldrich and Panreac. Ultrapure water from a Millipore Milli-Q system (resistivity > 18 MΩ cm) was employed to prepare all the aqueous solutions.

2.2. Synthesis of catalysts and manufacture of gas-diffusion cathodes

2.2.1. Synthesis of catalysts

First, MWCNTs were functionalized by the following chemical oxidation treatment in liquid phase [39]: reflux with concentrated HNO_3/H_2SO_4 2:3 (v/v) mixture at 80 °C for 0.5 h. After this treatment, the functionalized MWCNTs were always filtered, washed and dried.

The CoS_2-based catalysts were prepared following the procedure described by Dong et al. [40]. Briefly, $CoCl_2{\cdot}6H_2O$, $Na_2S_2O_3{\cdot}5H_2O$ and sulfur were mixed in molar proportion 2:2:1 in a PTFE autoclave of capacity 250 mL. To prepare supported catalysts, the synthesis was carried out in the presence of a certain amount of MWCNTs. Then, the autoclave was filled with ultrapure water, firmly closed and maintained at 140 °C for 24 h. Afterwards, the autoclave was cooled down to reach room temperature, and the solid obtained was filtered and washed several times with ultrapure water, ethanol and carbon sulfide. Finally, it was dried in an air oven at 80 °C. Catalysts thus prepared were denoted as CoS_2 black (unsupported nanoparticles) and CoS_2/MWCNT (supported nanoparticles).

2.2.2. Manufacture of gas-diffusion electrodes

Gas-diffusion electrodes consist of a catalyst layer and gas-diffusion layer. The spraying method was employed to manufacture the O_2- and air-diffusion cathodes of 36 cm^2 geometric area [41]. Selected catalysts were ultrasonically dispersed in 2-propanol and ultrapure water, with a molar ratio of 1:4, and Nafion® dispersion to form an ink. Then, the ink was sprayed in several steps onto the diffusion layer (Freudenberg H23C4, 255 μm thick) using an air-brush gun fed with pure nitrogen, and drying the material every time in an air oven at 60 °C for 20 min to obtain a GDE. The catalyst loading in the electrode was 2.0 mg cm^{-2} and the Nafion® content was 30 wt% (dry weight).

2.3. Surface and electrochemical characterization

The surface chemistry of raw and functionalized MWCNTs was analyzed by Temperature Programmed Desorption (TPD). The experiments were carried out using an Autochem II 2920 (Micromeritics) instrument, under Ar flow at 10 °C min^{-1} heating rate from 30 up to 1000 °C. The amounts of CO and CO_2 desorbed from the samples were analyzed by mass spectrometry. The peak deconvolution was performed according to references from Figueiredo et al. [42,43].

X-ray diffraction (XRD) analysis of the catalysts was made using a universal diffractometer Bruker D8 Advance, with Cu K_α radiation and a 2θ scan from 15 to 80° (at 1° min^{-1}). The average crystallite sizes were determined by the Scherrer equation, using the (200), (210) and (211) Bragg reflection peaks. Scanning electron microscopy (SEM) was performed with a JSM5910-LV JEOL microscope, whereas field emission SEM (FE-SEM) analysis was carried out using a Zeiss Ultra Plus microscope. Co:S atomic ratios were analyzed by energy dispersive X-ray (EDX) using an INCA-300 energy analyzer.

Textural properties of synthesized materials were determined with a Micromeritics ASAP 2020 porosimeter. N_2 adsorption-desorption over the CoS_2 and CoS_2/MWCNT samples at 77 K yielded the corresponding isotherms. Total Brunauer-Emmet-Teller (BET) surface areas and pore volumes of the samples were calculated by applying the BET equation and the single point method, respectively. The porosity distribution was determined using the N_2-DFT model.

X-ray photoelectron spectroscopy (XPS) technique was used to get information on the chemical state of surface species. The measurements were performed in a SPECS Sage HR 100 spectrometer with a non-monochromatic X-ray source of Mg with a Kα line of 1253.6 eV energy and 250 W. The samples were placed perpendicular to the analyzer axis and calibrated using the $3d_{5/2}$ line of Ag with a full width at half maximum (FWHM) of 1.1 eV. The selected resolution for the high resolution spectra was 15 eV of pass energy and 0.15 eV $step^{-1}$. Measurements were made in an ultra high vacuum (UHV) chamber at a pressure ca. 8×10^{-8} mbar. An electron flood gun was used to neutralize for charging. Asymmetric and Gaussian Lorentzian functions were used for the band deconvolution (after a Shirley background correction), constraining the FWHM of all peaks and setting free the peak positions and areas.

Cyclic and linear sweep voltammetries were registered using a PARSTAT 2273 potentiostat (Ametek, Inc.) driven by the PowerSuite software (version 2.58), in a conventional three-electrode glass cell thermostatized at 25 °C. Potentials were measured against a reversible hydrogen electrode, RHE (Gaskatel GmbH), in contact with the electrolyte through a tube ended in a Luggin capillary. The counter electrode was a platinum wire. The working electrode was a glassy carbon tip (0.07069 cm^2 geometric area) connected to a rotating disk electrode, RDE (model EDI101, Radiometer Analytical). The working electrode was prepared as follows: 1 mg of catalyst was dispersed in a 500 μL mixture of 2-propanol and deionized water (1:1 v/v) and sonicated for 0.5 h. An appropriate amount of this catalyst ink was transferred onto the surface of the glassy carbon disk. After gentle drying under N_2 stream, 5 μL of Nafion® (0.05 wt%) was dropped onto the catalyst layer to fix it, and to enlarge the electrode/electrolyte interface. In this way, the catalyst loading was 20 μg cm^{-2}. Prior to each analysis, glassy carbon disk was polished to a mirror finish using alumina powder suspensions (0.3 and 0.05 μm, Buehler, in that order), followed by sonication in water.

All the electrochemical measurements were performed with 50 mL of 0.050 M Na_2SO_4 (pH 3.0). The electrolyte was deaerated by bubbling nitrogen for 20 min prior to the experiments, and the inert atmosphere was maintained over the solution during the electrochemical analyses. Cyclic voltammetry signals were recorded at scan rate of 20 mV s^{-1}. Next, the saturation of the solution with pure O_2 was ensured by bubbling it for 30 min before the linear sweep voltammetry experiments. Then, *j-E* curves were recorded at rotation rates between 400 and 2500 rpm, and scan rate of 5 mV s^{-1}, to keep steady state conditions at the surface of the working electrode and to minimize the charging current. Current densities are given considering the geometrical area of the working electrode. All the *j-E* curves have been corrected by the IR-drop in the electrolyte solution, using the *eis* technique. The impedance spectra were collected from 100 kHz to 0.1 Hz at open circuit potential with amplitude of 5 mV.

2.4. Bulk electrolysis and analytical procedures

Galvanostatic bulk electrolyses for H_2O_2 electrogeneration and tetracaine degradation were performed in an open, undivided glass cell of 200 mL capacity, filled with 150 mL of solution under vigorous stirring provided by a magnetic PTFE follower, with a double jacket where thermostated water circulated at 35 °C. For the former assays, a 3-cm^2 dimensionally stable anode (IrO_2-based plate) purchased from NMT Electrodes (Pinetown, South Africa) was used, whereas for the latter ones the anode was a 3-cm^2 boron-doped diamond (BDD) thin-film plate supplied by NeoCoat (Le-Chaux-de-Fonds, Switzerland). The cathode was a 3-cm^2 GDE composed of carbon paper coated with the selected catalyst. It was mounted at the bottom of a polypropylene tube using the arrangement described elsewhere for a carbon-PTFE air-diffusion cathode [23], being fed with either pure O_2 at 0.2 barg and at flow rate of 0.5 L min^{-1} for H_2O_2 electrogeneration or air pumped at 1.0 L min^{-1} for decontamination trials. The gap between the anode and cathode was kept at 1 cm. All the assays were performed at a constant current density of 100 mA cm^{-2} controlled by an Amel 2049 potentiostat-galvanostat. The cell voltage was measured with a digital multimeter (Demestres 601BR). For comparison, H_2O_2 electrogeneration was also made under potentiostatic conditions at fixed E_{cat} without stirring. A similar setup was employed, including an Ag|AgCl (3 M KCl) reference electrode (Metrohm).

A 0.050 M Na_2SO_4 solution adjusted to pH 3.0 with H_2SO_4 was used in H_2O_2 electrogeneration trials. EO-H_2O_2 treatment of tetracaine was made with a 0.112 mM drug solution in 0.050 M Na_2SO_4 (pH 3.0). The same solution composition was employed for the PEF process, but adding 0.50 mM Fe^{2+} as catalyst and upon irradiation with a Philips TL/6 W/08 fluorescent black light blue tube. This UVA lamp was placed at 7 cm above the solution, emitting at λ_{max} = 360 nm with 5 W m^{-2} average power density, as measured with a Kipp & Zonen CUV 5 UV radiometer.

The solution pH was measured on a Crison GLP 22 pH-meter. The H_2O_2 concentration was obtained from the light absorption of its Ti(IV) complex at λ = 408 nm, measured on a Shimadzu 1800 UV/Vis spectrophotometer [36]. This approach is more reliable than rotating ring-disk electrode (RRDE) measurements to confirm the presence of H_2O_2. The solution TOC was determined by injecting 50 μL aliquots into a Shimadzu VCSN TOC analyzer. The tetracaine abatement was followed by reversed-phase high-performance liquid chromatography (HPLC) upon injection of 10 μL aliquots into a Waters 600 LC coupled with a Waters 996 photodiode array detector. The LC was fitted with a BDS Hypersil C18 (250 mm × 4.6 mm) column at room temperature, and a 50:50 (v/v) acetonitrile:water (KH_2PO_4 10 mM, pH 3.0) mixture was eluted at 1.0 mL min^{-1} as mobile phase. The tetracaine peak was detected at retention time of 8.9 min measured at λ = 311 nm.

3. Results and discussion

3.1. Physicochemical characterization of catalysts and supports

Considering the chemical inertness of raw MWCNTs, a first step prior to their use generally involves some kind of surface modification with the ability to impart functional groups to the carbon atom lattice. In general, such a pre-treatment allows a strong anchorage along with better dispersion of metal or metal oxide nanoparticles. As can be seen in Table 1, the chemical oxidative treatment of commercial MWCNTs

Table 1
Temperature programmed desorption (TPD) characterization of the raw and functionalized Arkema MWCNTs further used as support for CoS_2 particles.

Sample	Functional group/mol %						Total functional groups/μmol mg^{-1}	Degree of functionalization/wt%
	Carboxylic acid	Anhydride	Lactone	Phenol	Ether	Quinone		
Raw	3.8	1.7	0.2	42.3	23.6	28.3	0.6	1.8
Funct.	13.4	14.8	17.9	10.1	17.9	25.9	3.1	9.8

led to the appearance of oxygen-containing functionalities, mainly as carboxylic acid groups. The presence of these pending groups is thus essential for the subsequent preparation of inorganic/nanocarbon hybrids, since it allows the deposition of nanoparticles of smaller size with homogeneous dispersion onto the MWCNTs, as previously reported in the literature [44].

The synthesized CoS_2-based catalysts were characterized by XRD and FE-SEM techniques. Fig. 1 shows the X-ray diffraction patterns of both, the as-synthesized CoS_2 black particles and the supported catalyst (CoS_2/MWCNT). The patterns clearly show the (111), (200), (210), (211), (220), (311), (023), and (321) characteristic planes of cattierite (CoS_2) with a cubic phase (JCPDS No. 41-1471), confirming that both materials synthesized by one-pot hydrothermal method have crystalline structure. The peak at about $2\theta = 26^{\circ}$ in the diffractogram corresponding to CoS_2/MWCNT catalyst is associated with the (002) plane of the carbonaceous support material, although in this case the expected symmetry is broken by the presence of a complex structure of peaks on the right part. Such asymmetrical line may be attributed to the existence of different microstructures, as a result of carbon deviations from regular positions due to compaction during the synthesis step [45]. The average crystallite sizes were 24.2 and 19.7 nm for CoS_2 black and CoS_2/MWCNT catalysts, respectively. Worth mentioning, both values are lower than those reported in the literature for unsupported CoS_2 [21] and CoS_2-on-graphene catalysts [46], obtained by hydrothermal synthesis.

XPS analysis was used to characterize the oxidation states of the synthesized materials. Fig. S1a and b show the Co 2p and S 2p spectra corresponding to CoS_2 black, whereas those of the CoS_2/MWCNT catalyst are shown in Fig. S1c and d. The positions and relative intensities of the Co 2p and S 2p signals are in good agreement with previous results reported in the literature [20,47]. The Co $2p_{3/2}$ and $2p_{1/2}$ core level peaks are observed at binding energies of 779.2 and 794.4 eV, respectively (see Fig. S1a). Furthermore, the multiplet structure observed in the Co 2p high resolution spectra in both catalysts (see Fig. S1a and c) indicates that CoS_2 surface is susceptible to be oxidized in air

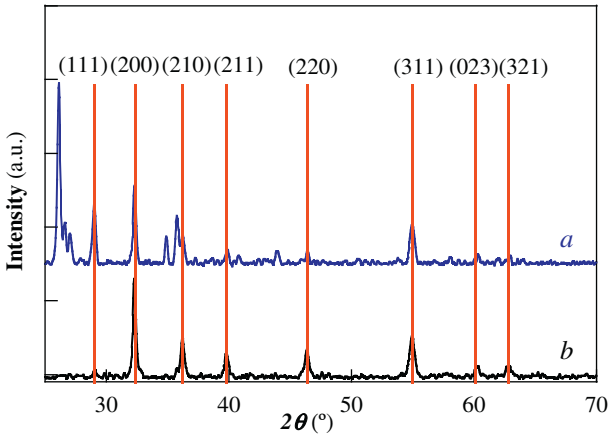

Fig. 1. X-ray diffractogram patterns of CoS_2-based catalysts: (*a*) CoS_2/MWCNT and (*b*) CoS_2 black for comparison. The red lines indicate the crystallographic planes of CoS_2. (For interpretation of the references to colour in this figure legend, the reader is referred to the web version of this article.)

[20]. This was supported by the presence of the sulfate peak at 168.8 eV in the S 2p spectra (see Fig. S1b and d). In those spectra, the signal at 163.1 eV is attributed to sulfide species [48]. Worth mentioning, the CoS_2 black reveals the presence of Co(0) apart from CoS_2. This signal is slightly weaker in CoS_2/MWCNT, which will require further investigation for clarification. In addition to previous profiles, the chemical composition (in at% of Co, S, C and O) was found to be 9.5%, 40.8%, 7.9% and 41.8% for CoS_2 black and 2.3%, 6.7%, 73.2% and 17.9% for CoS_2/MWCNT.

The morphology of the catalysts was characterized by FE-SEM. Nanocrystalline unsupported CoS_2 particles presented a cubic-like morphology, as can be observed in Fig. 2a. It is very important to note that such morphology is maintained in the supported catalyst (see Fig. 2b), where the presence of carbon nanotubes as underlying platform enhances considerably the CoS_2 dispersion, thus limiting the formation of particle aggregates. Furthermore, the atomic ratio Co:S determined by EDX was 1:2, in good agreement with the CoS_2 cattierite cubic phase identified from XRD analysis. In addition, the CoS_2 content

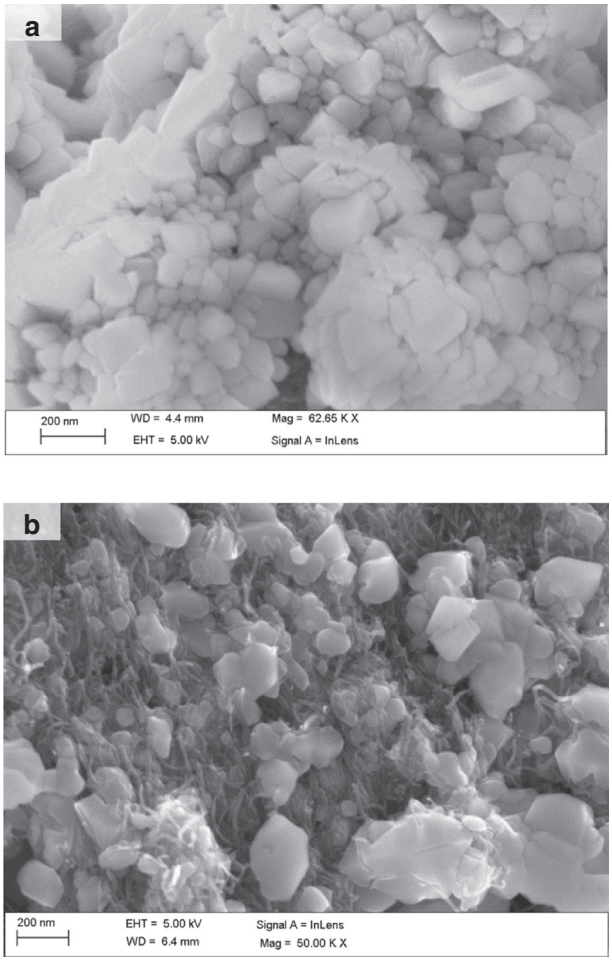

Fig. 2. FE-SEM images of (a) as-prepared CoS_2 black and (b) CoS_2/MWCNT.

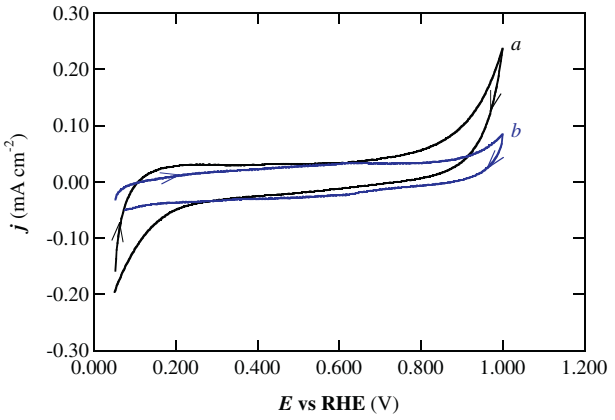

Fig. 3. Cyclic voltammograms recorded on (*a*) CoS_2 black and (*b*) CoS_2/MWCNT in N_2-saturated 0.050 M Na_2SO_4 solution at pH 3.0 and 25 °C. Scan rate 20 mV s^{-1}. Curves are IR-drop corrected.

in CoS_2/MWCNT catalyst was 46 wt%, closed to the expected nominal value of 50 wt%.

Table S1 summarizes the textural properties of the synthesized CoS_2-based materials. As can be seen, BET surface area corresponding to CoS_2/MWCNT was 8-fold higher than that of CoS_2 black. This huge difference could be attributed to the presence of carbon nanotubes in the supported electrocatalyst. In addition, from Table S1 it is evident that the specific volume of the pores was higher for CoS_2/MWCNT, in agreement with the morphology of both materials shown in Fig. 2. This can also be seen in the pore size distributions of the Fig. S2 included in the supplementary material.

3.2. Electrochemical characterization of catalysts

Cyclic voltammetry measurements were carried out for CoS_2 black and CoS_2/MWCNT catalysts in N_2-saturated aqueous solution of 0.050 M Na_2SO_4 at pH 3.0. Fig. 3 depicts the registered stable cyclic voltammograms for both catalysts (3th cycle), being the current densities expressed in terms of the geometrical surface area of the working electrode. The most relevant feature of both cyclic voltammograms is the double layer capacitance region that is extended from 0.200 to 0.800 V. The CoS_2 black catalyst exhibits a remarkable current increase at potentials higher than 0.800 V in the forward scan, and more negative in the backward, below 0.200 V (see curve *a* in Fig. 3). Ahlberg et al. [21] reported that the anodic current increase could be ascribed to the oxidation of disulfide to sulfate species, and the anodic dissolution of CoS_2, which can lead to the electrode degradation. The cathodic current has two components: one additional current increase that could be related to the reduction of an oxidized CoS_2 surface, only observed in the 1st cycle as shown in Fig. S3 (see also in Fig. S4 the comparison between Figs. 3 and S3), and the hydrogen evolution reaction. The most interesting feature, however, is that the presence of carbon nanotubes in the CoS_2/MWCNT catalyst seems to stabilize the CoS_2 nanoparticles, leading to an evident decrease of the mentioned faradaic processes (see curve *b* in Fig. 3). This is a very noteworthy consequence of the hybridization between the carbonaceous support and the metal sulfide, paving the way for the preparation of stable GDEs. Furthermore, the extension of the potential window, now working from − 0.200 to 1.200 V vs. RHE under the same experimental conditions as those of Fig. 3, allows the identification of the oxygen and hydrogen evolution reactions, which take place at potentials higher than 1.000 V and lower than 0.000 V vs. RHE, respectively, as shown in Fig. S5.

The oxygen reduction reaction on CoS_2 black and CoS_2/MWCNT catalysts was studied in aqueous 0.050 M Na_2SO_4 solution at pH 3.0 by linear sweep voltammetry, using an RDE setup. Fig. 4 shows the *j-E*

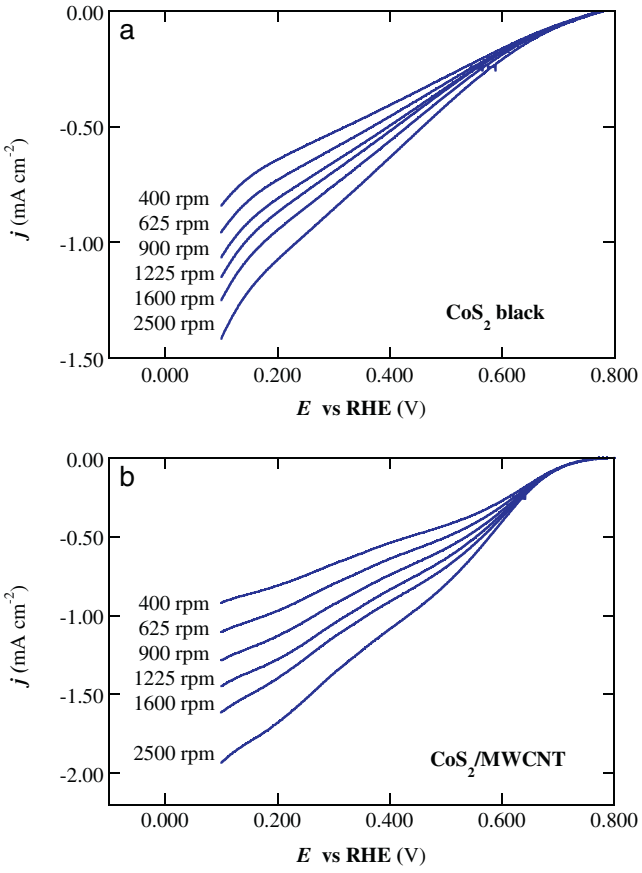

Fig. 4. Linear sweep voltammograms at different rotation rates in O_2-satured 0.050 M Na_2SO_4 solution at pH 3.0 and 25 °C corresponding to the following catalysts: (a) CoS_2 black and (b) CoS_2/MWCNT. Scan rate 5 mV s^{-1}. Curves are IR-drop corrected.

curves registered at different electrode rotating rates. From the curves in Fig. 4a and b, it is evident that both catalysts show activity towards the ORR. As the electrode rotation rate was increased, greater current densities for O_2 reduction were obtained, especially at less positive potentials and for the CoS_2/MWCNT catalyst. In addition, the half-wave potential ($E_{1/2}$) shifted qualitatively towards more negative potentials, which is indicative of a totally irreversible redox reaction. Furthermore, a closer inspection reveals that the shape of both groups of reduction *j-E* curves is different: those corresponding to the CoS_2 black catalyst show a unique wave (see Fig. 4a), whereas in the curves corresponding to the CoS_2/MWCNT catalyst the presence of two waves is deduced at about 0.800–0.400 and 0.400–0.100 V (see Fig. 4b). For comparison, the electrochemical behavior of MWCNT without CoS_2 is presented in Fig. S6, showing lower current densities than those observed for CoS_2/MWCNT in the entire range of potentials.

On the other hand, a Koutecky-Levich analysis was carried out to gain deeper insight into the kinetics of the ORR on these two catalysts. Fig. 5 shows the inverse of the current density (j^{-1}) at different applied potential values vs. the inverse of the square root of the rotation rates ($\omega^{-1/2}$), using the data extracted from the experimental curves plotted in Fig. 4. Linear fittings were obtained for CoS_2 black and CoS_2/MWCNT catalysts, and the straight lines were quite parallel to each other at the potentials considered, which confirms that the redox reaction is irreversible, as stated above. Even more relevant, the non-zero intercepts points towards kinetic limitations of the ORR on both catalysts (see Fig. 5a and b). As can be observed, higher *j* values were obtained with the supported catalyst at any given rotation rate, which can be partly related to its larger BET surface area (4.04 $m^2 g^{-1}$ for CoS_2 black vs. 32.5 $m^2 g^{-1}$ for CoS_2/MWCNT, see Table S1). The number of electrons, *n*, transferred per O_2 molecule was estimated from the slope

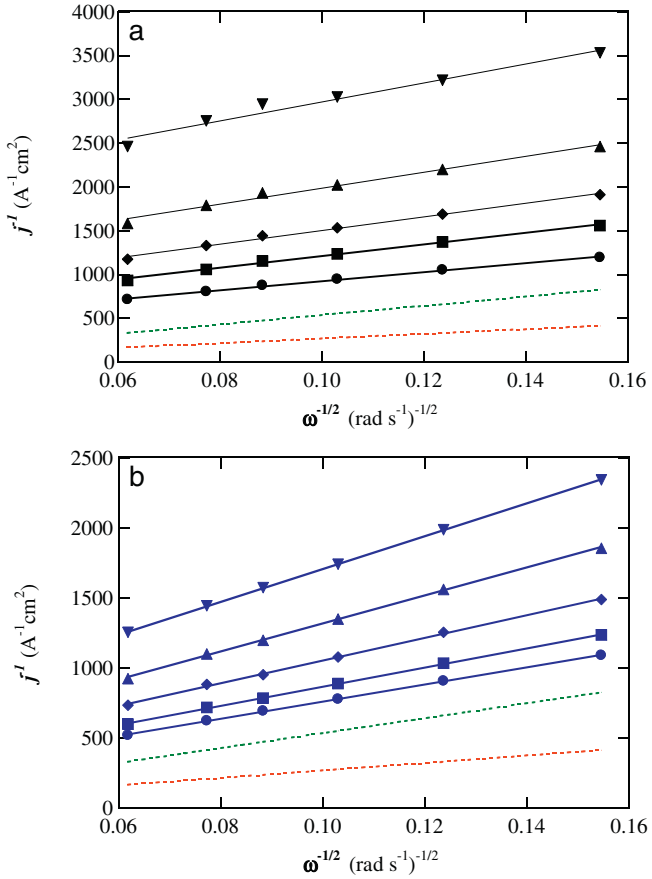

Fig. 5. Koutecky-Levich plots obtained from the data of Fig. 4 at different potentials for: (a) CoS_2 black and (b) CoS_2/MWCNT catalysts. Potentials: (●,●) 0.100 V, (■,■) 0.200 V, (◆,◆) 0.300 V, (▲,▲) 0.400 V and (▼,▼) 0.500 V. Theoretical plots for *n*: (---) 2 and (---) 4 have been included for comparison.

of the Koutecky-Levich plots of Fig. 5, using the following equation [49]:

$$\frac{1}{j} = \frac{1}{j_k} + \frac{1}{j_l} = \frac{1}{nFkC_{O_2}^b} + \frac{1}{0.62nFC_{O_2}^b D_{O_2}^{2/3} \upsilon^{-1/6} \omega^{1/2}} \quad (7)$$

where j is the measured current density, j_k the kinetic current density, j_l, the diffusion limiting current density, F is the Faraday constant (96,485.33 C mol^{-1}), k is the reaction rate constant, $C_{O_2}{}^b$ is the oxygen solubility (1.1×10^{-3} mol dm^{-3}), D_{O_2} is the O_2 diffusion coefficient (1.7×10^{-5} cm^2 s^{-1}), and υ is the kinematic viscosity of the solution (0.01 cm^2 s^{-1}). The numerical values of $C_{O_2}{}^b$, D_{O_2}, and υ have been extrapolated from data compiled in ref. [50], which are strictly applicable to an aqueous H_2SO_4 solution at pH = 3.0.

Table 2
Average number of electrons transferred (*n*) at different electrode potentials obtained for the ORR at several CoS_2-based catalysts from the slope of the Koutecky-Levich plots.

E vs. RHE (V)	*n*	
	CoS_2 black	CoS_2/MWCNT
0.500	1.1	1.0
0.400	1.3	1.2
0.350	1.4	1.3
0.300	1.6	1.5
0.250	1.7	1.6
0.200	1.8	1.8
0.150	2.0	1.9
0.100	2.3	2.0

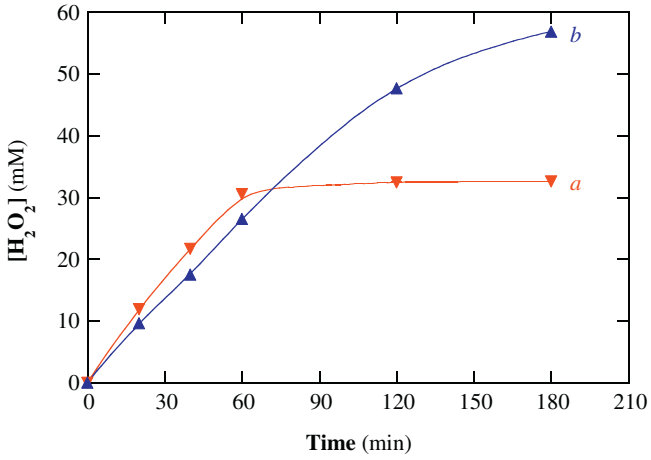

Fig. 6. Time course of H_2O_2 concentration accumulated in 150 mL of 0.050 M Na_2SO_4 at pH 3.0 and 35 °C using an undivided cell with an IrO_2-based anode and an air-diffusion cathode, both of 3 cm^2 area, at constant current density of 100 mA cm^{-2}. The cathode contained: (*a*) MWCNT, and (*b*) CoS_2/MWCNT, always using functionalized MWCNTs.

Table 2 summarizes the *n* values obtained for the CoS_2 black and CoS_2/MWCNT catalysts at different potentials. At low applied potentials ($E < 0.200$ V), the true value of *n* is 2 for both catalysts, given that numerical values of $C_{O_2}{}^b$, D_{O_2} and υ used in Eq. (7) are approximate. This confirms the ability of such CoS_2-based catalyst to form H_2O_2 as the final product. This finding agrees with the behavior of some cobalt sulfide for which the two-electron ORR is the dominant reaction pathway, especially at specific cathodic *E* values [46]. Note that, for comparison, Fig. 5 includes the theoretical j^{-1} vs. $\omega^{-1/2}$ lines that should be expected supposing an *n* of 2 (reduction of O_2 to H_2O_2) or 4 (reduction to H_2O), clearly showing that the slope of the Koutecky-Levich plots gradually tended to match with the plot for $n = 2$.

3.3. Bulk electrolyses using the manufactured gas-diffusion electrodes

From a technical point of view, it is crucial not only to investigate the ability of a given material to produce H_2O_2, as shown in Section 3.2, but also to demonstrate the feasibility of long-term H_2O_2 electrogeneration in acidic medium under galvanostatic conditions, since this is the most widespread operation mode in systems that include gas-diffusion cathodes for water treatment. With this purpose, two gas-diffusion electrodes were manufactured as explained in Subsection 2.2.2, based on either functionalized MWCNTs or CoS_2/MWCNT catalyst. Preparative electrolyses were carried out in 150 mL of 0.050 M Na_2SO_4 at pH 3.0 and 35 °C using an undivided cell with an IrO_2-based anode and an air-diffusion cathode, both of 3 cm^2 area, at constant current density of 100 mA cm^{-2}. Fig. 6 depicts the time course of H_2O_2 concentration accumulated for 180 min. A quick rise in the H_2O_2 content was found for both cathodes within the first 60 min, reaching about 30 mM H_2O_2, which corresponds to 82% current efficiency. This is a very high value, taking into account that in an undivided cell part of the produced H_2O_2 is continuously destroyed by oxidation at the anode surface according to consecutive reactions (8) and (9) [4]:

$$M + H_2O_2 \rightarrow M(HO_2^{\bullet}) + H^+ + e^- \quad (8)$$

$$M(HO_2^{\bullet}) \rightarrow M + O_2 + H^+ + e^- \quad (9)$$

Hence, the functionalized MWCNTs are shown as an optimum carbonaceous support for H_2O_2 electrogeneration, since a lower amount has been usually reported under analogous conditions using commercial GDEs based on carbon black particles with PTFE as binder material [4,36].

A second remarkable feature of Fig. 6 is the very different profile of both curves from 60 min. In the setup equipped with the non-catalyzed

(curve *a*) GDE, the H_2O_2 concentration almost achieved a steady state (32 mM H_2O_2 at 180 min), suggesting that the generation rate at the cathode from reaction (1) became equal to its destruction rate via reactions (8) and (9). This is an evidence of the loss of electrocatalytic ability of the cathode and/or a poorer stability upon prolonged electrolysis, ending in a smaller relative ratio at which the ORR occurs, in favor of the four-electron reduction reaction. This explanation agrees with the radically different performance of the catalyzed GDE. For this cathode, a gradual increase of the H_2O_2 content was found for 180 min, attaining 56.9 mM H_2O_2 without showing the aforementioned plateau. This means that the CoS_2 particles had a preeminent role for enhancing the two-electron ORR, which can be explained from two standpoints: (i) they may promote the formation of H_2O_2 within a certain potential range (Fig. 4a and Table 2), and (ii) they might stabilize the MWCNTs surface against chemical degradation.

Once the high performance of the CoS_2/MWCNT air-diffusion cathode in terms of H_2O_2 production was ascertained, its ability to be applied to EAOPs like EO-H_2O_2 and PEF was tested for the anaesthetic tetracaine. This organic compound is an emerging water pollutant that has been detected in hospital wastewater at an average concentration of 0.48 μg L^{-1} [51]. Comparative experiments were performed with 150 mL of 0.112 mM of the drug in 0.050 M Na_2SO_4 at pH 3.0 and 35 °C using an undivided cell with a 3 cm^2 BDD anode and a 3 cm^2 CoS_2/MWCNT GDE for 180 min at 100 mA cm^{-2}. No significant change of solution pH was found during the trials. Note that, using this kind of

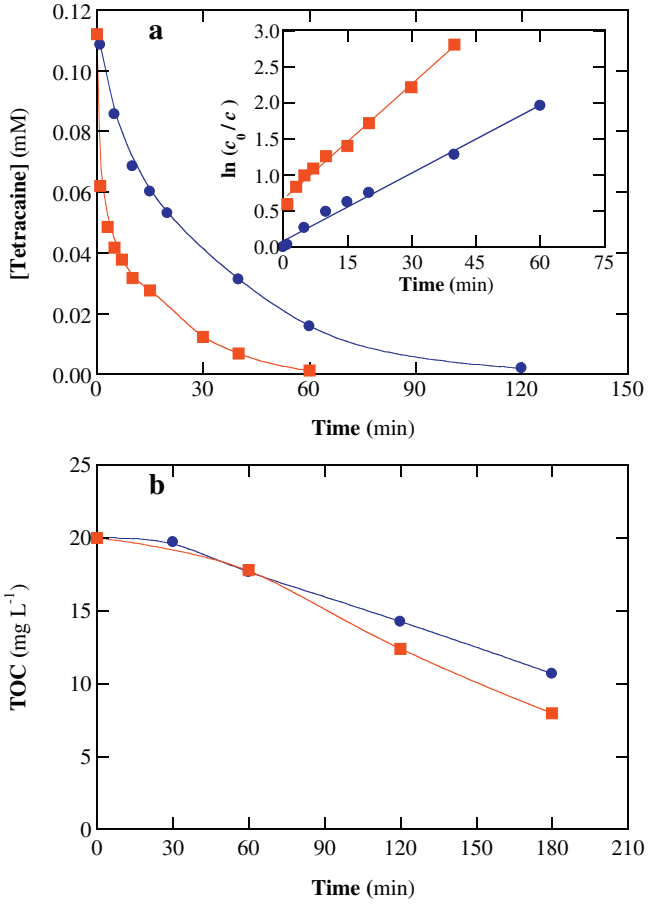

Fig. 7. (a) Tetracaine concentration decay and (b) TOC removal vs. electrolysis time for the degradation of 150 mL of 0.112 mM drug solutions in 0.050 M Na_2SO_4 at pH 3.0 and 35 °C using an undivided cell with a 3 cm^2 boron-doped diamond (BDD) anode and a 3 cm^2 carbon paper modified with CoS_2/MWCNT as air-diffusion cathode, at current density of 100 mA cm^{-2}. Method: (●) electrochemical oxidation with electrogenerated H_2O_2 (EO-H_2O_2) and (■) photoelectro-Fenton (PEF) with 0.50 mM Fe^{2+} using a 6 W UVA lamp. The inset panel presents the pseudo-first-order kinetics from the analysis of the drug decay.

catalyst, a more environmentally sustainable water treatment technology is obtained compared to those based on unsupported catalysts because the final separation from the treated effluent is not required.

Fig. 7a highlights a more rapid exponential decay of tetracaine concentration using PEF than EO-H_2O_2. The drug disappeared in 120 min using the latter EAOP, which was mainly due to the attack of generated BDD(˙OH) from reaction (2) because blank trials revealed the insignificant oxidation power of H_2O_2 on this drug. In contrast, it was removed in a shorter time of 60 min in PEF with 0.50 mM Fe^{2+} upon UVA irradiation with a 6 W lamp, as a result of the additional formation of oxidant ˙OH in the bulk from Fenton's reaction (3) and the photolytic reaction (5). The inset panel of Fig. 7a shows the good linear correlation obtained assuming a pseudo-first-order kinetics for the drug abatement by the EO-H_2O_2 process, yielding an apparent rate constant (k_1) of 0.031 min^{-1} with R^2 = 0.990. For PEF, however, this inset highlights that a pseudo-first-order kinetics was only verified for reaction times > 3 min, with k_1 = 0.054 min^{-1} and R^2 = 0.992, because of the dramatic decay of drug concentration during the first stage of the treatment. This behavior could be explained by a change in the electroactive species of tetracaine along electrolysis time, as found for other *N*-aromatics [52]. In particular, the fast generation of Fe^{3+} ion from Fenton's reaction (3) could give rise to a Fe(III)-tetracaine complex as the main form of the drug to be destroyed from 3 min of electrolysis. This complex is more stable and hence, it reacts much more slowly than the parent tetracaine molecule present at the beginning of the treatment. The pseudo-first-order decay of the drug concentration found in both methods suggests its reaction with a steady concentration of hydroxyl radicals (BDD(˙OH) and/or ˙OH).

Fig. 7b depicts the TOC abatement for the trials shown in Fig. 7a. A larger final mineralization with 60% TOC reduction can be observed for PEF, whereas the EO-H_2O_2 process only led to 43% TOC removal at 180 min. The superiority of PEF can be ascribed to the faster destruction of contaminants by generated ˙OH and photolysis of Fe(III)-carboxylate complexes from reactions (3), (5) and (6). All these reactions are concomitant to that involving BDD(˙OH), which is the single powerful oxidant in EO-H_2O_2.

The above results regarding tetracaine degradation corroborate the excellent behavior of the manufactured CoS_2/MWCNT GDE as cathode to be used in EAOPs based on Fenton's reaction chemistry.

4. Conclusions

Hydrothermally synthesized CoS_2 black and CoS_2/MWCNT catalysts were composed of cubic cattierite (CoS_2, atomic ratio Co:S of 1:2) nanocrystals with size of 24.2 and 19.7 nm, respectively. The presence of functionalized carbon nanotubes rich in oxygen-containing functionalities as support enhanced very significantly the dispersion and stability of CoS_2 particles, giving rise to viable CoS_2-based inorganic/nanocarbon composites. Both catalysts showed activity towards the ORR, prevailing the two-electron pathway at low applied potentials (E < 0.200 V). The ability of the supported CoS_2-based catalyst to form H_2O_2 as the final product in acidic medium was proven by means of galvanostatic bulk electrolyses using purpose-made GDEs. At 180 min, contents of 32.0 and 56.9 mM H_2O_2 were attained with the non-catalyzed and the CoS_2/MWCNT GDE, respectively. Total removal of the pharmaceutical tetracaine from an acidic aqueous solution was achieved in 60 or 120 min by PEF and EO-H_2O_2 with a BDD anode at 100 mA cm^{-2}, attaining 60% and 43% TOC removal at 180 min, respectively.

Acknowledgements

Financial support from projects CTQ2013-48897-C2-1-R and CTQ2013-48897-C2-2-R (MINECO/FEDER, EU) and CTQ2016-78616-R (AEI/FEDER, EU), as well as from excellence network E3TECH under project CTQ2015-71650-RDT (MINECO, Spain) is acknowledged. The

FPI grant awarded to C. Ridruejo (MINECO, Spain) is also acknowledged.

Appendix A. Supplementary data

Supplementary data to this article can be found online at http://dx.doi.org/10.1016/j.jelechem.2017.09.010.

References

[1] A.S. Martins, T.C.R. Ferreira, R.L. Carneiro, M.R.V. Lanza, Simultaneous degradation of hexazinone and diuron herbicides by H_2O_2/UV and toxicity assessment, J. Braz. Chem. Soc. 25 (2014) 2000–2006.
[2] J.J. Pignatello, E. Oliveros, A. MacKay, Advanced oxidation processes for organic contaminant destruction based on the Fenton reaction and related chemistry, Crit. Rev. Environ. Sci. Technol. 36 (2006) 1–84.
[3] J.M. Campos-Martín, G. Blanco-Brieva, J.L.G. Fierro, Hydrogen peroxide synthesis: an outlook beyond the anthraquinone process, Angew. Chem. Int. Ed. 45 (2006) 6962–6984.
[4] E. Brillas, I. Sirés, M.A. Oturan, Electro-Fenton process and related electrochemical technologies based on Fenton's reaction chemistry, Chem. Rev. 109 (2009) 6570–6631.
[5] K.V. Plakas, A.J. Karabelas, S.D. Sklari, V.T. Zaspalis, Toward the development of a novel electro-Fenton system for eliminating toxic organic substances from water. Part 1. In situ generation of hydrogen peroxide, Ind. Eng. Chem. Res. 52 (2013) 13948–13956.
[6] Q. Li, C. Batchelor-McAuley, N.S. Lawrence, R.S. Hartshorne, C.V.J. Jones, R.G. Compton, A flow system for hydrogen peroxide production at reticulated vitreous carbon via electroreduction of oxygen, J. Solid State Electrochem. 18 (2014) 1215–1221.
[7] G. Coria, T. Pérez, I. Sirés, J.L. Nava, Mass transport studies during dissolved oxygen reduction to hydrogen peroxide in a filter-press electrolyzer using graphite felt, reticulated vitreous carbon and boron-doped diamond as cathodes, J. Electroanal. Chem. 757 (2015) 225–229.
[8] F. Yu, M. Zhou, X. Yu, Cost-effective electro-Fenton using modified graphite felt that dramatically enhanced on H_2O_2 electro-generation without external aeration, Electrochim. Acta 163 (2015) 182–189.
[9] J.F. Pérez, J. Llanos, C. Sáez, C. López, P. Cañizares, M.A. Rodrigo, Electrochemical jet-cell for the in-situ generation of hydrogen peroxide, Electrochem. Commun. 71 (2016) 65–68.
[10] G.R. Agladze, G.S. Tsurtsumia, B.-I. Jung, J.-S. Kim, G. Gorelishvili, Comparative study of hydrogen peroxide electro-generation on gas-diffusion electrodes in undivided and membrane cells, J. Appl. Electrochem. 37 (2007) 375–383.
[11] C. Flox, J.A. Garrido, R.M. Rodríguez, P.L. Cabot, F. Centellas, C. Arias, E. Brillas, Mineralization of herbicide mecoprop by photoelectro-Fenton with UVA and solar light, Catal. Today 129 (2007) 29–36.
[12] M. Giomo, A. Buso, P. Fier, G. Sandonà, B. Boye, G. Farnia, A small-scale pilot plant using an oxygen-reducing gas-diffusion electrode for hydrogen peroxide electrosynthesis, Electrochim. Acta 54 (2008) 808–815.
[13] W.R.P. Barros, T. Ereno, A.C. Tavares, M.R.V. Lanza, In situ electrochemical generation of hydrogen peroxide in alkaline aqueous solution by using an unmodified gas diffusion electrode, ChemElectroChem 2 (2015) 714–719.
[14] X. Yu, M. Zhou, G. Ren, L. Ma, A novel dual gas diffusion electrodes system for efficient hydrogen peroxide generation used in electro-Fenton, Chem. Eng. J. 263 (2015) 92–100.
[15] J.F. Carneiro, R.S. Rocha, P. Hammer, R. Bertazzoli, M.R.V. Lanza, Hydrogen peroxide electrogeneration in gas diffusion electrode nanostructured with Ta_2O_5, Appl. Catal. A Gen. 517 (2016) 161–167.
[16] W.R.P. Barros, P.C. Franco, J.R. Steter, R.S. Rocha, M.R.V. Lanza, Electro-Fenton degradation of the food dye amaranth using a gas diffusion electrode modified with cobalt (II) phthalocyanine, J. Electroanal. Chem. 722–723 (2014) 46–53.
[17] W.R.P. Barros, S.A. Alves, P.C. Franco, J.R. Steter, R.S. Rocha, M.R.V. Lanza, Electrochemical degradation of tartrazine dye in aqueous solution using a modified gas diffusion electrode, J. Electrochem. Soc. 161 (2014) H867–H873.
[18] M.-R. Gao, J. Jiang, S.-H. Yu, Solution-based synthesis and design of late transition metal chalcogenide materials for oxygen reduction reaction (ORR), Small 8 (2012) 13–27.
[19] Y. Liang, Y. Li, H. Wang, H. Dai, Strongly coupled inorganic/nanocarbon hybrid materials for advanced electrocatalysis, J. Am. Chem. Soc. 135 (2013) 2013–2036.
[20] M.S. Faber, R. Dziedzic, M.A. Lukowski, N.S. Kaiser, Q. Ding, S. Jin, High-performance electrocatalysis using metallic cobalt pyrite (CoS_2) micro- and nanostructures, J. Am. Chem. Soc. 136 (2014) 10053–10061.
[21] J. Jirkovský, A. Björling, E. Ahlberg, Reduction of oxygen on dispersed nanocrystalline CoS_2, J. Phys. Chem. C 116 (2012) 24436–24444.
[22] L. Feng, E.D. van Hullebusch, M.A. Rodrigo, G. Esposito, M.A. Oturan, Removal of residual anti-inflammatory and analgesic pharmaceuticals from aqueous systems by electrochemical advanced oxidation processes. A review, Chem. Eng. J. 228 (2013) 944–964.
[23] I. Sirés, E. Brillas, M.A. Oturan, M.A. Rodrigo, M. Panizza, Electrochemical advanced oxidation processes: today and tomorrow. A review, Environ. Sci. Pollut. Res. 21 (2014) 8336–8367.
[24] B. Boye, P.A. Michaud, B. Marselli, M.M. Dieng, E. Brillas, C. Cominellis, Anodic oxidation of 4-chlorophenoxyacetic acid on synthetic boron-doped diamond electrodes, New Diamond Front. Carbon Technol. 12 (2002) 63–72.
[25] C. Flox, P.L. Cabot, F. Centellas, J.A. Garrido, R.M. Rodríguez, C. Arias, E. Brillas, Electrochemical combustion of herbicide mecoprop in aqueous medium using a flow reactor with a boron-doped diamond anode, Chemosphere 64 (2006) 892–902.
[26] A. Thiam, E. Brillas, F. Centellas, P.L. Cabot, I. Sirés, Electrochemical reactivity of Ponceau 4R (food additive E124) in different electrolytes and batch cells, Electrochim. Acta 173 (2015) 523–533.
[27] A. Thiam, I. Sirés, J.A. Garrido, R.M. Rodríguez, E. Brillas, Decolorization and mineralization of Allura Red AC aqueous solutions by electrochemical advanced oxidation processes, J. Hazard. Mater. 290 (2015) 34–42.
[28] I. Sirés, E. Brillas, Remediation of water pollution caused by pharmaceutical residues based on electrochemical separation and degradation technologies: a review, Environ. Int. 40 (2012) 212–229.
[29] M. Haidar, A. Dirany, I. Sirés, N. Oturan, M.A. Oturan, Electrochemical degradation of the antibiotic sulfachloropyridazine by hydroxyl radicals generated at a BDD anode, Chemosphere 91 (2013) 1304–1309.
[30] A. El-Ghenymy, R.M. Rodríguez, E. Brillas, N. Oturan, M.A. Oturan, Electro-Fenton degradation of the antibiotic sulfanilamide with Pt/carbon-felt and BDD/carbon-felt cells. Kinetics, reaction intermediates, and toxicity assessment, Environ. Sci. Pollut. Res. 21 (2014) 8368–8378.
[31] M. Panizza, A. Dirany, I. Sirés, M. Haidar, N. Oturan, M.A. Oturan, Complete mineralization of the antibiotic amoxicillin by electro-Fenton with a BDD anode, J. Appl. Electrochem. 44 (2014) 1327–1335.
[32] N. Barhoumi, L. Labiadh, M.A. Oturan, N. Oturan, A. Gadri, S. Ammar, E. Brillas, Electrochemical mineralization of the antibiotic levofloxacin by electro-Fenton-pyrite process, Chemosphere 141 (2015) 250–257.
[33] A. Özcan, A.A. Özcan, Y. Demirci, Evaluation of mineralization kinetics and pathway of norfloxacin removal from water by electro-Fenton treatment, Chem. Eng. J. 304 (2016) 518–526.
[34] T. Pérez, I. Sirés, E. Brillas, J.L. Nava, Solar photoelectro-Fenton flow plant modeling for the degradation of the antibiotic erythromycin in sulfate medium, Electrochim. Acta 228 (2017) 45–56.
[35] A. El-Ghenymy, R.M. Rodríguez, C. Arias, F. Centellas, J.A. Garrido, P.L. Cabot, E. Brillas, Electro-Fenton and photoelectro-Fenton degradation of the antimicrobial sulfamethazine using a boron-doped diamond anode and an air-diffusion cathode, J. Electroanal. Chem. 701 (2013) 7–13.
[36] G. Coria, I. Sirés, E. Brillas, J.L. Nava, Influence of the anode material on the degradation of naproxen by Fenton-based electrochemical processes, Chem. Eng. J. 304 (2016) 817–825.
[37] C. Salazar, C. Ridruejo, E. Brillas, J. Yáñez, H.D. Mansilla, I. Sirés, Abatement of the fluorinated antidepressant fluoxetine (Prozac) and its reaction by-products by electrochemical advanced methods, Appl. Catal. B Environ. 203 (2017) 189–198.
[38] Y. Lin, J. Yu, Z. Xing, X. Guo, X. Yu, B. Tang, J. Zou, Enhanced generation of H_2O_2 and radicals on Co_9S_8/partly-graphitized carbon cathode for degradation of bio-refractory organic wastewater, Electrochim. Acta 213 (2016) 341–350.
[39] L. Calvillo, M. Gangeri, S. Perathoner, G. Centi, R. Moliner, M.J. Lázaro, Effect of the support properties on the preparation and performance of platinum catalysts supported on carbon nanofibers, J. Power Sources 192 (2009) 144–150.
[40] J. Dong, D. Li, Z. Peng, Y. Zhou, Synthesis and electrochemical performance of cobalt disulfide, J. Solid State Electrochem. 12 (2008) 171–174.
[41] G. Álvarez, F. Alcaide, P.L. Cabot, M.J. Lázaro, E. Pastor, J. Solla-Gullón, Electrochemical performance of low temperature PEMFC with surface tailored carbon nanofibers as catalyst support, Int. J. Hydrog. Energy 37 (2012) 393–404.
[42] J.L. Figueiredo, M.F.R. Pereira, M.M.A. Freitas, J.J.M. Órfão, Modification of the surface chemistry of activated carbons, Carbon 37 (1999) 1379–1389.
[43] J.L. Figueiredo, M.F.R. Pereira, The role of surface chemistry in catalysis with carbons, Catal. Today 150 (2010) 2–7.
[44] L. Han, W. Wu, F.L. Kirk, J. Luo, M.M. Maye, N.N. Kariuki, Y. Lin, C. Wang, C.J. Zhong, A direct route toward assembly of nanoparticle – carbon nanotube composite materials, Langmuir 20 (2004) 6019–6025.
[45] Z.Q. Li, C.J. Lu, Z.P. Xia, Y. Zhuo, Z. Luo, X-ray diffraction patterns of graphite and turbostatic carbon, Carbon 45 (2007) 1686–1695.
[46] H. Wang, Y. Liang, Y. Li, H. Dai, $Co_{1-x}S$-graphene hybrid: a high-performance metal chalcogenide electrocatalyst for oxygen reduction, Angew. Chem. Int. Ed. 50 (2011) 10969–10972.
[47] Y. Liu, B. Zhao, Y. Zhang, H. Zhang, K. Zhan, J. Yang, J. Li, Co supported catalysts on nitrogen and sulfur co-doped vertically-aligned carbon nanotubes for oxygen reduction reaction, RSC Adv. 6 (2016) 32676–32684.
[48] D.C. Higgins, F.M. Hassan, M.H. Seo, J.Y. Choi, M.A. Hoque, D.U. Lee, Z. Chen, Shape-controlled octahedral cobalt disulfide nanoparticles supported on nitrogen and sulfur doped graphene/carbon nanotube composites for oxygen reduction in acidic electrolyte, J. Mater. Chem. A 3 (2015) 6340–6350.
[49] C. Du, Q. Tan, G. Yin, J. Zhang, Rotating disk electrode method, in: W. Xing, G. Yin, J. Zhang (Eds.), Rotating Electrode Methods and Oxygen Reduction Electrocatalysts, Elsevier, Amsterdam, 2014, pp. 171–198.
[50] W. Xing, M. Yin, Q. Lv, Y. Hu, C. Liu, J. Zhang, Oxygen solubility, diffusion coefficient, and solution viscosity, in: W. Xing, G. Yin, J. Zhang (Eds.), Rotating Electrode Methods and Oxygen Reduction Electrocatalysts, Elsevier, Amsterdam, 2014, pp. 1–31.
[51] B.I. Escher, R. Baumgartner, M. Koller, K. Treyer, J. Lienert, C.S. McArdell, Environmental toxicology and risk assessment of pharmaceuticals from hospital wastewater, Water Res. 45 (2011) 75–92.
[52] F. Gozzi, I. Sirés, A. Thiam, S.C. de Oliveira, A. Machulek Jr., E. Brillas, Treatment of single and mixed pesticide formulations by solar photoelectro-Fenton using a flow plant, Chem. Eng. J. 310 (2017) 503–513.